This is a repository copy of *A modified synchronverter for a weak grid with virtual power circles-based PQ decoupling scheme*.

White Rose Research Online URL for this paper:
https://eprints.whiterose.ac.uk/218632/

Version: Published Version

Article:

ORIGINAL RESEARCH

A modified synchronverter for a weak grid with virtual power circles-based PQ decoupling scheme

Daniel Angelo Kisinga[1] | **Peter Makolo**[2] | **Paul Trodden**[1]

[1]Department of Automatic Control & Systems Engineering, University of Sheffield, Sheffield, UK

[2]Department of Electrical Engineering, University of Dar es Salaam, Dar es Salaam, Tanzania

Correspondence
Daniel Angelo Kisinga, Department of Automatic Control, and Systems Engineering, University of Sheffield, Sheffield, UK.
Email: kisingadaniel@gmail.com

Abstract

The high penetration of renewable energy sources (RES) results in a low-inertia, weak power grid. To mitigate this and restore system inertia, it has been widely proposed to operate the inverters of RES units to mimic synchronous generators; this technology is known as a virtual synchronous generator (VSG). In weak grids there is, however, strong coupling between active power (P) and reactive power (Q), and any VSG technique therefore requires PQ decoupling in order to operate effectively. This article proposes a new PQ decoupling technique based on the transformation of the PQ power circle of a VSG connected to a weak grid: first, the power circle is *translated* from its designed position to that of a conventional synchronous generator (SG) connected to a *strong* grid, achieving *partial PQ* decoupling. Then, to achieve full PQ decoupling, the authors propose further to modulate the radius of the translated PQ power circle; this is achieved using a series resistance-capacitance–inductance (*RCL*) circuit which is virtually implemented in the VSG controller. The efficacy of the proposed scheme is validated using a modified synchronverter connected to the weak grid in representative loading scenarios. It is demonstrated that the technique achieves a decoupled PQ control for the synchronverter connected in a weak grid. Moreover, the modified synchronverter is capable of supporting frequency and voltage regulation in the grid without inducing large transient grid currents during mild frequency and voltage variations.

1 | INTRODUCTION

1.1 | Motivation

The penetration of renewable energy sources (RES) into electrical power systems (EPS) is projected to increase from 25% in 2021 to 90% in 2050 [1]. Inertia-less sources—such as Wind Turbine Generation (WTG) and Solar Photovoltaic Systems (SPV)—are expected to contribute the majority of that increase; the net effect will be large-scale reductions in system inertia [2, 3]. Inertia provides the first line of defence against frequency contingencies in an EPS and its decline may result in an increased rate of change of frequency (RoCoF) and excessive frequency deviations in response to contingencies. Such deviations may trigger special protection schemes such as RoCoF and Under-Frequency Load Shedding (UFLS) relays, and even lead to cascading failures and blackouts [4].

To increase the inertia of an EPS with high penetration of RES units, an interfacing power electronic converter (inverter) can be controlled to mimic the operation of a synchronous generator (SG). This technology is known as a *virtual synchronous generator* (VSG). The concept was first introduced by Becke and Hesse in 2007 [5] and has seen numerous improvements and modifications since; current designs and topologies of VSGs include the virtual synchronous machine (VISMA) [5], the synchronverter [6], the simplified swing equation-based VSG [7], reactive-power frequency-based VSG [8], a de-loaded active power-based VSG [9] and droop-based VSG [10]. Studies have indicated that, among these designs, the synchronverter may be the most effective in limiting RoCoF and frequency nadir in low-inertia systems [11]. One of the outstanding challenges for synchronverter technology is, however, how to achieve decoupling of the active (P) and reactive power (Q) [6]; in the original development of the technology, the synchronverter was

connected to a *strong* grid and thus, the *PQ* coupling effect was not recognized appreciably.

The *PQ* decoupling problem is particularly timely because the increasing penetration of RES into electrical power systems is accompanied by an associated decrease in the short circuit level (SCL) [12] and, thus, an overall *weakening* of the grid. WTG and SPV systems, for example, generate short-circuit fault currents in the order of one-fifth of those for large coal and gas-fired units [13]. A decrease of SCL signifies an increase in the resistive component of the grid, which results in a resistive or inductive–resistive system. Hence, a weak grid is characterized by a low X/R ratio [14]. In these weak grids, P and Q have a strong coupling effect which requires an effective *PQ* decoupling technique for their independent control. The aim of this article is, therefore, to develop a simple and practical *PQ* decoupling scheme for a synchronverter connected to a weak grid.

1.2 | Related work

Various approaches have been proposed in the literature to solve the *PQ* decoupling problem, as surveyed in the sequel. In [15] a novel linearization-based *PQ* control scheme is proposed to reduce oscillations caused by *PQ* coupling. The method requires a parametric value (m)—the tangent of the *PQ* circle—which is difficult to estimate and compute. The scheme in [16] feeds forward reference values for P and Q, determined from a small-signal model of the VSG; despite the simplicity of obtaining the controller gains, determination of the required increments to power angle and internal voltage of the VSG can be complex to determine in practice. In [17] a virtual impedance is designed based on the capacitor current feedback for suppression of the harmonics, while quantification of the required magnitude of the virtual impedance is done on the basis of the modulation signal. The relationship between coupling of the *PQ* and the virtual impedance is, however, not investigated. In [18] the idea of using virtual negative resistance to achieve *PQ* decoupling, proposed in [19], is enhanced to mimic a proportional–resonant controller in its implementation. Practical applicability may be limited, however, by the observation that use of a proportional integral (PI) controller in the voltage control loop may lead to critical stability of the DC components of the output currents; moreover, the VSG structure was not considered in the design of the controller of the inverter. In [20] a novel non-phase locked loop (PLL) based method for *PQ* control with Hilbert transform is proposed. The method does not, however, incorporate the VSG structure in the inverter control design. In [21, 22] a modified PLL is proposed: P and Q are decoupled based on the axial voltages, achieved by the addition of a series virtual inductance. However, quantification of magnitude of the virtual inductance is needed and its effect on the system is not investigated.

Virtual impedance has been used in the VSG design for limiting fault currents, improving power sharing, and suppressing harmonic oscillations. In [23] a large virtual impedance is designed to limit the symmetrical three phase fault currents in the microgrid. Motivated by this work, [24] improved the output

impedance of the synchronverter by adding a large virtual inductance in series with the stator inductance. The added inductance is intended to increase stability of the synchronverter by preventing the occurrence of undesirable large current variations in the event of the small-to-mild grid voltage variations. The use of large voltage impedance, however, increases the voltage drop which can hinder power transfer; moreover, in [24] the synchronverter is connected to a strong grid and hence the *PQ* coupling effect is not studied. In [25] a finite control set model predictive control-based VSG is designed for an islanded microgrid, wherein a virtual impedance is used to shape the output impedance of the converter for accurate power sharing. In this work, however, the quantification of the required magnitude of the virtual impedance is not provided. In [26] a coordinated virtual impedance based control is proposed for a three-phase four-leg inverter to mitigate harmonics and achieve power sharing. The work, however, does not specify the type and quantities of the required virtual impedances. Moreover, no inertia emulation is considered in the proposed inverter. On the other hand, in [17, 27, 28] the virtual impedance is quantified based on the harmonic analysis to improve the harmonic oscillations of the current. A virtual impedance with fractional proportional integral derivative (PID) controller is used to achieve accurate reactive power sharing in [29], while in [30] adaptive virtual impedance is used in a microgrid to achieve the same goal. In all of the latter, analysis is limited to the case of an islanded microgrid. Moreover, quantification of the virtual impedance is limited to a particular application, whether harmonic analysis or reactive power sharing. This results in complexity in sizing of the values of virtual impedance.

1.3 | Contribution

The *PQ* decoupling problem remains an open challenge with practical implications; this is in particularly true for VSG technologies connected to a weak grid, where *PQ* coupling is stronger. While the use of the virtual impedance shows promise, the quantification of its required magnitude remains challenging.

This article, therefore, proposes a simple *PQ* decoupling scheme for a VSG connected to a weak grid. The scheme is based on *shifting* of the power circle of the VSG and *modulation* of its radius via the addition of virtual impedance; that is, the power circle of the VSG is first translated to a location similar to that of an SG connected to a *strong* grid and then, based on the power rating of the VSG, a desired *PQ* circle is achieved by modulation of its radius. This provides a clear link between desired *PQ* circle and the necessary virtual impedance. Hence, the magnitude of the virtual impedance is easily quantified from the centre and radius of the desired location of the virtual power circle.

To demonstrate the efficacy of the proposed scheme, a modified synchronverter is designed and connected to a weak grid, and it is shown that the proposed scheme can achieve a satisfactorily decoupled *PQ* control. Moreover, it is shown that the supplied grid currents adhere to the IEEE 1547 standard—such that the total harmonic distortion (THD) is less than 5%—and
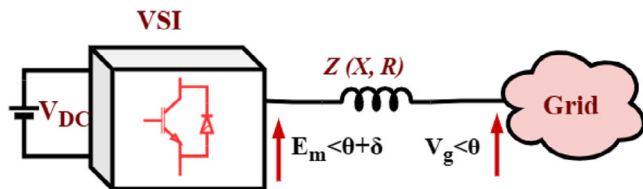
FIGURE 1 A simplified block diagram of a synchronverter connected to the grid.

that the synchronverter aids recovery of nominal frequency and voltage levels without producing large grid currents.

1.4 | Organization

The rest of this article is organized as follows. Section 2 starts by outlining the power transfer theory between a synchronverter and the grid and identifying the PQ coupling effect of a weak grid. The section goes on to explain the proposed concept of virtual shifting of the PQ power circle, including the working principle of the proposed scheme in order to achieve partial decoupling, and then modifications to achieve further, adequate decoupling. Section 3 introduces the synchronverter model and defines guidelines for its virtual component sizing. Section 4 is devoted to the practical implementation of the proposed scheme. Simulation results and conclusions are provided in Sections 5 and 6, respectively.

2 | A PQ DECOUPLING SCHEME FOR A SYNCHRONVERTER CONNECTED TO A WEAK GRID

2.1 | Power transfer theory and the PQ coupling effect

A synchronverter transfers power from a RES unit, or dedicated energy storage source (ESS) unit, to the grid. At synchronization this is equivalent to the power transfer between an AC source and the grid; Figure 1 illustrates a synchronverter as an AC voltage source synchronized to the power grid, separated by an equivalent complex impedance $Z(X, R)$. The real and reactive powers transferred to the grid are [31]

$$P = \frac{3V_g E_m}{2|Z|} \cos(\alpha - \delta) - \frac{3V_g^2}{2|Z|} \cos \alpha, \quad (1)$$

$$Q = \frac{3V_g E_m}{2|Z|} \sin(\alpha - \delta) - \frac{3V_g^2}{2|Z|} \sin \alpha, \quad (2)$$

where V_g and θ are the amplitude and angle, respectively, of the grid voltage V, and E_m and $\theta + \delta$ are the amplitude and angle of the internal voltage (E) of the VSG. Hence, δ is the power angle; that is, the difference of angles between E and V.
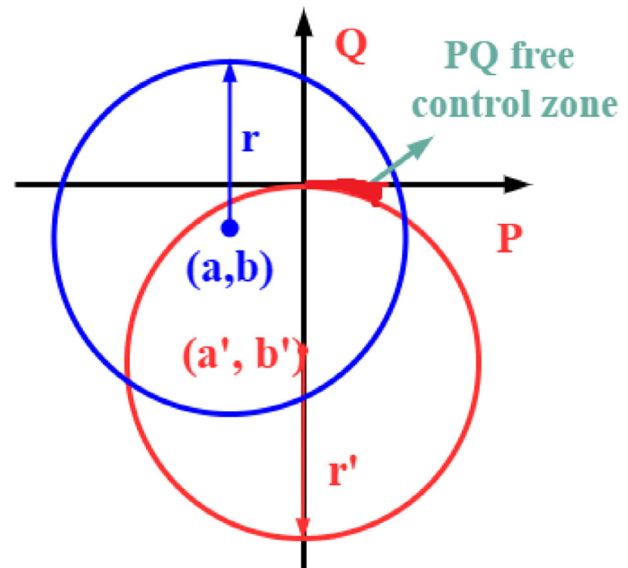
FIGURE 2 PQ power circles for a VSG connected to a weak grid (blue circle) and an SG connected to a strong grid (red circle).

Equations (1) and (2) can be combined to form a PQ circle

$$\left(P + \frac{3V_g^2}{2|Z|}\cos\alpha\right)^2 + \left(Q + \frac{3V_g^2}{2|Z|}\sin\alpha\right)^2 = \left(\frac{3V_g E_m}{2|Z|}\right)^2, \quad (3)$$

whose centre coordinates (a, b) are

$$a = -\frac{3V_g^2 R}{2(X^2 + R^2)}, \qquad b = -\frac{3V_g^2 X}{2(X^2 + R^2)}, \quad (4)$$

and whose radius (r) is

$$r = \frac{3V_g E_m}{2\sqrt{X^2 + R^2}}. \quad (5)$$

In a weak grid, X and R are approximately equal or with relatively small differences [14]. Hence, the PQ circle for a VSG connected to a weak grid is similar to the blue circle shown in Figure 2, that is, such that $a < 0$ and $b < 0$ with $a \approx b$. The consequence of this is that P and Q are typically strongly coupled around the operating point of the VSG: controlled changes to $P > 0$ result into uncontrolled changes to Q.

In contrast, the connection of a conventional SG to a strong, highly inductive grid results in P and Q being largely decoupled. Let $Z_s(X_s, R_s)$ denote the impedance between the SG and the strong grid. The conventional SG operates with a value of α close to $90°$, such that

$$P = \frac{3V_g E_m}{2X_s}\sin\delta, \quad (6)$$

$$Q = \frac{3V_g}{2X_s}\left(E_m\cos\delta - V_g\right), \quad (7)$$

which may be combined to give the PQ circle

$$(P)^2 + \left(Q + \frac{3V_g^2}{2X_s}\right)^2 = \left(\frac{3V_g E_m}{2X_s}\right)^2. \qquad (8)$$

The coordinates of the centre of this circle are

$$d' = 0, \qquad b' = -\frac{3V_g^2}{2X_s}, \qquad (9)$$

while the radius is

$$r' = \frac{3V_g E_m}{2X_s}. \qquad (10)$$

This circle is indicated in red on Figure 2. There exists a small portion of the circle—the shaded region labelled the *PQ free control zone*—where P and Q are nearly decoupled: a $P > 0$ can be provided by varying δ while Q remains near to zero or, more precisely, within a tolerable range. At the same time, desired a non-zero value of Q can be transferred to the grid at near-constant P by making variations to the internal voltage amplitude E_m. Hence, in this region of operation, a decoupled PQ control can be achieved.

2.2 | Working principle of the proposed scheme: Partial decoupling

The aim is to achieve decoupled PQ control for the synchronverter connected to a weak grid, and to achieve this in such a way that P and Q may be controlled using conventional methods; that is, direct power angle (δ) control for P and internal voltage amplitude (E_m) modulation for Q. To achieve this aim, the PQ power circle of the VSG connected to the weak grid will be shifted to a location corresponding to that of an SG connected to a strong grid, as indicated in Figure 2. To this end, the first step is to translate the centre of the PQ power circle from (a, b) to (d', b'). This requires the P-coordinate of the power circle to be moved from $a \neq 0$ to $d' = 0$. From (4), $a = 0$ if and only if $R = 0$ since $V_g > 0$ is enforced by the grid. To achieve this, therefore, we propose to add a virtual resistance $R_v = -R$ in series with the original impedance $Z(X, R)$. The subsequent total equivalent interfacing resistance seen by the system, $R_T = R_v + R$, will then be equal to zero.

This shifts the P-coordinate of the power circle's centre to $a = d' = 0$ but also modifies the radius r to

$$r = \frac{3V_g E_m}{2\sqrt{X^2 + R_T^2}} = \frac{3V_g E_m}{2\sqrt{X^2}}. \qquad (11)$$

Hence, in order to maintain the radius at its original value, a virtual inductive impedance X_{L_v} is added. Thus, the total equivalent interfacing impedance is

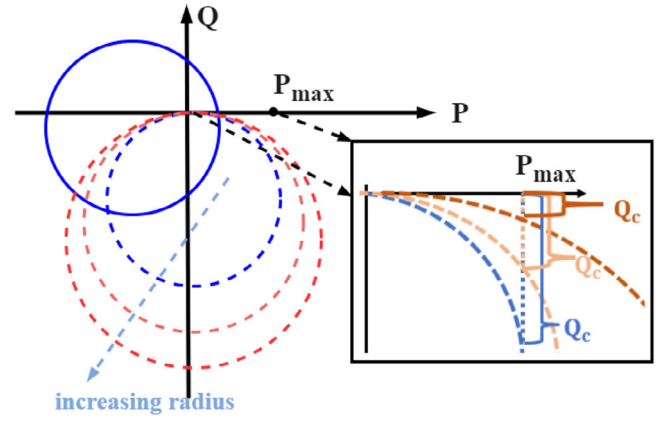$$Z_T(X_T, R_T) = \underbrace{(R + R_v)}_{R_T=0} + j\underbrace{(X + X_{L_v})}_{X_T}, \qquad (12)$$

FIGURE 3 Conceptual visualization of how the PQ circles can be translated and modulated to achieve satisfactory decoupling of P and Q.

yielding the radius

$$r = \frac{3V_g E_m}{2\sqrt{X_T^2 + R_T^2}} = \frac{3V_g E_m}{2(X + X_{L_v})}, \qquad (13)$$

and Q-coordinate of the circle's centre

$$b = -\frac{3V_g^2}{2(X + X_{L_v})}. $$

Note that this circle passes through the point $(0,0)$ if $E_m = V_g$. Moreover, if

$$X_{L_v} = \sqrt{X^2 + R^2} - X, \qquad (14)$$

then

$$r = \frac{3V_g E_m}{2\sqrt{X^2 + R^2}} \quad \text{and} \quad b = \frac{3V_g^2}{2\sqrt{X^2 + R^2}}, \qquad (15)$$

and the circle has the original radius of (5); furthermore,

$$r = \frac{E_m}{V_g}b \quad \text{and} \quad r - b = \frac{3V_g}{2\sqrt{X^2 + R^2}}\left(E_m - V_g\right). \qquad (16)$$

The net effect of the addition of the series impedance $Z_v(X_{L_v}, R_v)$ is therefore to translate the PQ power circle of the weak grid-connected synchronverter to resemble that of an equal-sized SG connected to a strong grid.

2.3 | An analysis of PQ coupling

This translation does not necessarily achieve adequate decoupling of P and Q, since the PQ free control zone is limited in extent if the power circle radius is small. This is illustrated in Figure 3, where the solid blue circle is the original one of the weak grid-connected synchronverter and the dashed blue circle is the resulting PQ following the addition of $Z_v(X_{L_v}, R_v)$. We present an analysis of this coupling in this section, leading to

conditions on the circle radius that must be satisfied to achieve adequate decoupling.

Suppose that it is desired to supply $(P, Q) = (P_{\text{ref}}, Q_{\text{ref}})$. Following the translation describe in the previous section, the P and Q supplied are, in terms of the circle radius r and Q-centre b,

$$P = r \sin \delta \qquad (17)$$

$$Q = r \cos \delta - b. \qquad (18)$$

Three facts are apparent from these relations:

1) $P = P_{\text{ref}}$ is possible only if $r \geq P_{\text{ref}}$; the value of δ required to provide $P = P_{\text{ref}}$ is then

$$\delta_{\text{ref}} = \sin^{-1} \frac{P_{\text{ref}}}{r} \in \left[-\pi/2, +\pi/2 \right]. \qquad (19)$$

2) $Q = Q_{\text{ref}}$ with $P = 0$ can be achieved by setting

$$r - b = \frac{3V_g}{2\sqrt{X^2 + R^2}} \left(E_m - V_g \right) = Q_{\text{ref}}. \qquad (20)$$

3) If $r - b = Q_{\text{ref}}$ to provide $Q = Q_{\text{ref}}$, then setting $\delta = \delta_{\text{ref}}$ in order to achieve $P = P_{\text{ref}}$ results in

$$Q = Q_{\text{ref}} - Q_c(r), \qquad (21)$$

where

$$Q_c(r) := r(1 - \cos \delta_{\text{ref}}) = r \left(1 - \sqrt{1 - \left(\frac{P_{\text{ref}}}{r} \right)^2} \right). \qquad (22)$$

This means that supplying $P = P_{\text{ref}}$ via control of δ is accompanied by a coupled reactive power Q_c that perturbs from the reference value Q_{ref} (including when $Q_{\text{ref}} = 0$); this coupled perturbation $Q_c(r)$ is, for $r \geq P_{\text{ref}}$, a monotonically decreasing function of r such that:

1) $Q_c(r) = P_{\text{ref}}$ when $r = P_{\text{ref}}$;
2) $Q_c(r) \to 0$ as $r \to \infty$;
3) $Q_c(r_2) < Q_c(r_1)$ for $r_2 > r_1$.

To reduce this coupling the radius of the power circle must therefore be increased. It is shown in Figure 3 that as the radius of the circle increases the magnitude of Q_c decreases and, thus, the extent of the PQ free control zone increases. It is also evident that there exists a circle for which $P = P_{\text{ref}}$ is possible while $|Q_c| \leq \varepsilon$, for any positive constant ε; in particular, solving (22) with the condition $|Q_c| \leq \varepsilon$ yields

$$r \geq \frac{P_{\text{ref}}^2 + \varepsilon^2}{2\varepsilon}. \qquad (23)$$

The problem of providing $P = P_{\text{ref}}$ and $Q = Q_{\text{ref}} - Q_c$ with $|Q_c| \leq \varepsilon$ is then (theoretically) just a matter of selecting a

sufficiently large radius of the circle; however, setting $X_{Lv} = \sqrt{X^2 + R^2} - X$ as described in the previous section provides no guarantee that (23) is met.

2.4 | Modifications to achieve adequate decoupling

It can be observed from (13) that to increase the radius requires the reactance $X + X_{Lv}$ to decrease, since E_m is reserved for Q control while V_g is the grid voltage. To achieve this a capacitor with reactance X_v is added in series with the original interfacing inductance X. The new interfacing reactance is

$$X'_T = X + X_{Lv} + X_v, \qquad (24)$$

where—if $X_{Lv} = \sqrt{X^2 + R^2} - X$, as previously explained—X_v may be sized such that

$$X'_T = \gamma \sqrt{X^2 + R^2}, \qquad (25)$$

with $0 < \gamma \leq 1$ because the value of X_v is negative.

This results in the radius

$$r(\gamma, E_m) = \frac{r_0(E_m)}{\gamma} \quad \text{where} \quad r_0(E_m) := \frac{3V_g E_m}{2\sqrt{X^2 + R^2}}, \qquad (26)$$

where we now explicitly notate that r is a function of γ and E_m. This replaces condition (23) with

$$\frac{r_0(E_m)}{\gamma} \geq \frac{P_{\text{ref}}^2 + \varepsilon^2}{2\varepsilon} \iff \gamma \leq \frac{2\varepsilon}{P_{\text{ref}}^2 + \varepsilon^2} \frac{3V_g E_m}{2\sqrt{X^2 + R^2}}. \qquad (27)$$

Likewise, the corresponding centre coordinates are $a = 0$ and

$$b(\gamma) = \frac{b_0}{\gamma} \quad \text{where} \quad b_0 := -\frac{3V_g^2}{2\sqrt{X^2 + R^2}}. \qquad (28)$$

This replaces condition (20) with

$$\frac{3V_g}{2\gamma\sqrt{X^2 + R^2}} \left(E_m - V_g \right) = Q_{\text{ref}}. \qquad (29)$$

Now it is seen that problem of providing $P = P_{\text{ref}}$ and $Q = Q_{\text{ref}} - Q_c$ with $|Q_c| \leq \varepsilon$ is a matter of setting the virtual reactance and finding a suitable pair (E_m, γ) such that (27) and (29) are met. Motivated by this, we define the following algorithm for selecting the virtual circuit parameters.

Algorithm 1 (*PQ* Decoupling Scheme). *Given* $P_{\text{ref}}, Q_{\text{ref}}, V_g, R, X$ *and* ε

1) *Obtain* γ *by solving the optimization problem*

$$\max_{\gamma, E_m} \left\{ \gamma : (27), (29), E_m^{\min} \leq E_m \leq E_m^{\max}, \gamma \leq 1 \right\}. \qquad (30)$$
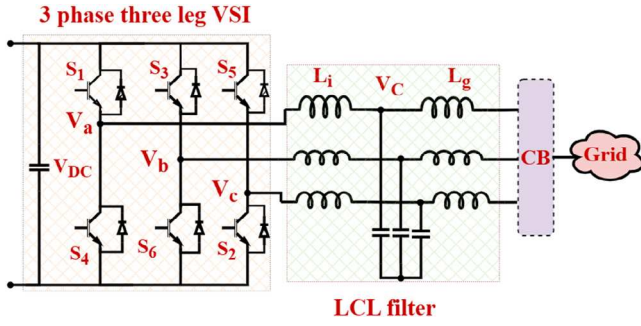
FIGURE 4   A general configuration of the grid connected synchronverter.

2) Set the virtual resistance $R_v = -R$ and virtual reactance $X_{Lv} + X_v$ as

$$X_{Lv} = \sqrt{X^2 + R^2} - X \qquad (31)$$

$$X_v = (\gamma - 1)\sqrt{X^2 + R^2}. \qquad (32)$$

Algorithm 1 selects the virtual circuit parameters such that the power circle passes through the points $(P, Q) = (0, Q_{ref})$ and $(P, Q) = (\pm P_{ref}, Q_{ref} - Q_c)$, with $|Q_c| \leq \varepsilon$, for some $E_m \in \left[E_m^{min}, E_m^{max}\right]$. The maximal γ is taken to maintain the interfacing impedance as large possible while satisfying the developed conditions on power supply and PQ decoupling; a smaller γ implies the need for a larger capacitance in series with the interfacing impedance, and a small system impedance may lead to large transient current values during faults.

3 | MODELLING AND COMPONENT SIZING OF THE SYNCHRONVERTER

3.1 | Modelling of the synchronverter

A synchronverter is an inverter that mimics the operation of a synchronous generator; a typical circuit diagram is given in Figure 4. In this article, we consider—similar to [6]—that the synchronverter mimics a round rotor non-salient machine with no damper windings, no magnetic saturation, no eddy current losses and one pair of magnetic poles.

On the electrical side, the machine is composed of the internal voltage (E), armature resistance (R_s) and inductance (L_s), and terminal voltage (V_t), related as

$$E = L_s \frac{dI}{dt} t + I R_s + V_t, \qquad (33)$$

where θ is the grid voltage angle, δ is the power angle, and I is the supplied current. The internal voltage E is controlled by the excitation of the machine. For a three-phase system with $I = (I_a, I_b, I_c)$ and $V_t = (V_{ta}, V_{tb}, V_{tc})$, the internal phase

voltages $E = (E_a, E_b, E_c)$ are

$$\begin{cases} E_a = E_m \sin(\theta + \delta), \\ E_b = E_m \sin\left(\theta - \frac{2\pi}{3} + \delta\right), \\ E_c = E_m \sin\left(\theta - \frac{4\pi}{3} + \delta\right), \end{cases} \qquad (34)$$

where $E_m = K_T \omega_v$, with K_T an excitation constant from the voltage control loop, and ω_v is the virtual frequency of the synchronverter. The latter is governed by the swing equation,

$$J_v \frac{d\omega_v}{dt} = \frac{P_{mec}}{\omega} - \frac{P}{\omega} - D(\omega_v - \omega), \qquad (35)$$

where J_v is the virtual inertia constant, ω is the nominal grid frequency, P_{mec} is the mechanical input power, and P is the power supplied to the grid:

$$P = E_m I_a \sin(\theta + \delta) + E_m I_b \sin\left(\theta - \frac{2\pi}{3} + \delta\right) \\ + E_m I_c \sin\left(\theta - \frac{4\pi}{3} + \delta\right), \qquad (36)$$

with corresponding reactive power

$$Q = -E_m I_a \cos(\theta + \delta) - E_m I_b \cos\left(\theta - \frac{2\pi}{3} + \delta\right) \\ - E_m I_c \cos\left(\theta - \frac{4\pi}{3} + \delta\right). \qquad (37)$$

3.2 | The virtual stator-component sizing

The output voltage of the VSI contains harmonics which hinder its direct synchronization with the grid; these harmonics distort the voltage profile and impose high reactive power requirements on the power system operator (PSO). According to IEEE 1547 [32], the supplied current into the grid must have harmonic content less than 5%. Therefore, a low-pass filter is required to ensure harmonic requirements are met; the *LCL* filter offers a favourable solution here in terms of the harmonic attenuation per unit cost and size [33], and is therefore designed for interfacing the VSI with the grid.

In the current context the *LCL* filter forms the stator of the synchronverter, and thus its sizing is of great importance. To achieve accurate sizing the algorithms proposed in [34–36] are combined, with some modifications, accounting for the following considerations.

- The power transfer between two synchronized sources is limited by the size of the interfacing impedance between them. If P_r is the rating of the synchronverter, the maximum impedance between the grid and synchronverter is

$$|Z|_{max} = \frac{3 V_g E_m^{max}}{2 P_r}. \qquad (38)$$

The total interfacing impedance, once the *LCL* filter is added, must therefore not exceed this value.

- The resonant frequency of the *LCL* filter is

$$f_{\text{res}} = \frac{1}{2\pi} \sqrt{\frac{L_i + L_g}{C_f L_i L_g}}, \tag{39}$$

where L_i is the inverter side inductance, L_g is the grid side inductance and C_f is the filter capacitance. This frequency must be within a specified range,

$$10 f_0 \leq f_{\text{res}} \leq 0.5 f_s, \tag{40}$$

where f_0 is the power frequency and f_s is the switching frequency, since resonance below this range adversely affects power frequency operations, while resonance higher than this range affects system sampling and switching of the VSI.

Therefore (38) and (40) form two general conditions that must be adhered to while sizing the filter for the grid connected VSI.

3.2.1 | Sizing of the inverter side inductor (L_i)

The size of the inverter side inductance is determined on the basis of the allowed current ripple of the supplied current to the grid. Considering a three-phase–three-leg VSI, the supplied current ripple is

$$\Delta I = \frac{2V_{\text{DC}}}{L_i} m(1 - m) T_s, \tag{41}$$

where V_{DC} is the DC link voltage of the VSI, m is the modulation index, T_s is the switching cycle period and ΔI is the ripple in the current supplied. The maximum supplied current ripple, attained with $m = 0.5$, is

$$\Delta I_{\text{max}} = \frac{V_{\text{DC}}}{6 L_i f_s}. \tag{42}$$

However, the relation between maximum current I_{max}, rated phase voltage V_p, and rated power P_r is

$$I_{\text{max}} = \frac{\sqrt{2} P_r}{3 V_p}. \tag{43}$$

Therefore, if the allowed maximum current ripple is $\Delta I_{\text{max}} = \kappa I_{\text{max}}$, then

$$L_i = \frac{V_{\text{DC}} V_p}{2\sqrt{2} \kappa f_s P_r}, \tag{44}$$
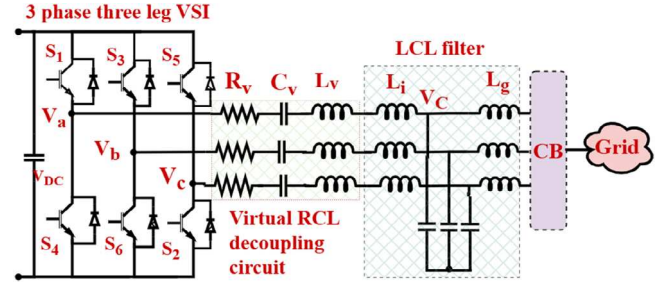
is the required inverter side inductance.

FIGURE 5 A modified synchronverter with *RCL*-decoupling circuit.

3.2.2 | Sizing of the grid side inductor (L_g)

The size of L_g is related to L_i by a parametric value r:

$$L_i = r L_g. \tag{45}$$

According to [34], the maximum harmonic attenuation is obtained when $r = 1$ and, thus, the values of L_i and L_g should be equal.

3.2.3 | Sizing of the *LCL*-filter capacitance (C_f)

The size of the capacitor affects the power factor and voltage profile of the synchronverter. Moreover, its value is also affected by, and inversely related to, the value of L_i. That is, if there is a large L_i, a small capacitance is sufficient to ensure higher harmonics attenuation. In [36, 37], C_f was sized to limit the reduction power factor to 5%. Hence,

$$C_f = 0.05 C_b, \tag{46}$$

where

$$C_b = \frac{1}{2\pi f_0 |Z|_{\text{max}}}. \tag{47}$$

From extensive simulations results and considering the dependency between L_i and f_s, however, it was found that a more effective sizing of C_f is

$$C_f = \frac{0.05}{2\pi f_0 |Z_L|}, \tag{48}$$

where

$$|Z_L| = 2\pi f_0 (L_i + L_g). \tag{49}$$

4 | IMPLEMENTATION OF THE PROPOSED *PQ* DECOUPLING SCHEME

The final implementation of the proposed scheme requires the addition of an *RCL*-decoupling circuit, as shown in Figure 5; this figure provides only a symbolic representation, because the *RCL*-decoupling circuit is implemented virtually in the controller of the synchronverter. The virtual implementation of the
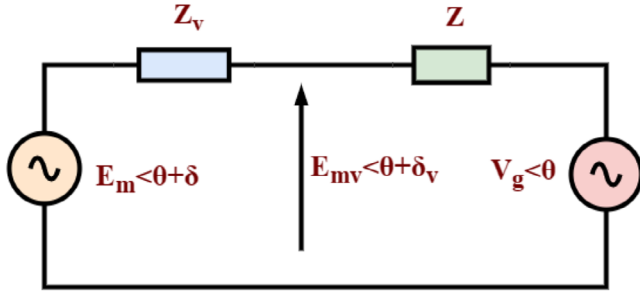
FIGURE 6 Impedance model of the grid connected inverter with a series virtual impedance.

TABLE 1 System parameters.

Parameter	Value
Rated power (P_r)	5 kW
DC bus voltage (V_{DC})	700 V
Phase voltage (V_p)	240 V
C_f	50 ⁻F
$L_i = L_g$	5 mH
X/R ratio	1.05
T_s	40 ⁻s
D_p	5000
D_q	50
κ	0.1

decoupling circuit minimizes the cost of implementation and ensures sustainable control; that is, it eliminates the need for re-configuring the hardware part of the synchronverter should the P requirement vary or the grid weaken.

The *RCL*-decoupling circuit modifies (33) to

$$E = \int \frac{I}{C_v} \, dt + (L_v + L_i)\frac{dI}{dt} + I(R_s + R_v) + V_t. \quad (50)$$

The magnitude of L_v is computed from X_{Lv}, while that of C_v is evaluated on basis of the value of γ, which, as previously explained, is selected based on the reference power (P_{ref}, Q_{ref}). To obtain the reference powers, droop controllers are used:

$$P_{ref} = P_{set} + D_p(\omega - \omega_v), \quad (51)$$

$$Q_{ref} = Q_{set} + D_q(V_{ref} - V_g), \quad (52)$$

where D_p is the droop gain for the P–ω control in the system and D_q is the droop gain for the Q–V control. From the reference powers and selected value of γ, C_v is quantified and hence the required magnitude of the virtual impedance. Moreover, the required magnitude of the internal voltage (E_m) and power angle (δ) can be computed from the P and Q equations using X'_T. The synchronverter controller (SC) is, however, modified where the input to the modulator is virtual power angle (δ_v) and virtual amplitude of the internal voltage (E_{mv}). These values are computed from the impedance model of the grid connected inverter, given in Figure 6. Based on this model, the values of δ_v and E_{mv} can be calculated. Thus, contrary to [38], direct power-angle control of the synchronverter is deployed which offers simplicity in tuning of the parameters due to the removal of the PI controller.

5 | SIMULATION RESULTS

Figure 7 provides a per-phase representation of a simplified grid-connected synchronverter system used for simulation studies. The system parameters are as provided in Table 1. The system is implemented and simulated in MATLAB/SIMULINK.

Five cases are demonstrated to test the validity of the proposed *PQ* decoupling scheme. The first case verifies the *PQ* coupling that exists when a synchronverter is connected to a weak grid without any decoupling technique. The second case shows that there exists a partial *PQ* decoupling when a synchronverter *PQ* power circle is virtually moved to the location similar to the SG connection to the grid ($\gamma = 1$). The third case demonstrates that satisfactory *PQ* decoupling is achieved with $\gamma = 0.04$. Then, the fourth and fifth cases are the extensions of the third case, where the synchronverter under the proposed scheme is shown to aid the grid during mild frequency and voltage variations. This is achieved without causing large undesired grid currents. In all the cases, the system is initialized and the circuit breaker is turned ON at 0.5 s to synchronize the inverter to the grid.

5.1 | Operation on the actual *PQ*-power circle

Figure 8 provides simulation results for this case. Referring to Figure 3, this case is similar to trying to control P and Q independently on the solid blue circle. Thus, no virtual impedance is used and, hence, there is no quantification of γ. A system is initialized and synchronised to the grid at around 0.5 s. Then, while Q is kept constant, a step change in P is demanded at 1 s. It is observed that the measured P follows the reference value (P_{set}), but Q also changes, undesirably deviating away from its setpoint. Hence, there exists a strong coupling between P and Q and therefore a decoupling technique is required to achieve independent P and Q control.

5.2 | Operation on the shifted virtual PQ-power circle ($\gamma = 1$)

This is similar to controlling P and Q on the dotted blue circle of Figure 3. Hence, the radius of the actual *PQ* power circle and shifted virtual *PQ* power circle are the same. Thus, the total impedance ($Z_T(X_T)$) of the shifted virtual *PQ* power circle is equal to the original interfacing impedance ($Z(X, R)$) between the synchronverter and the grid. The proposed scheme is tested under three step changes of P, that is from 0 to 1000 W at
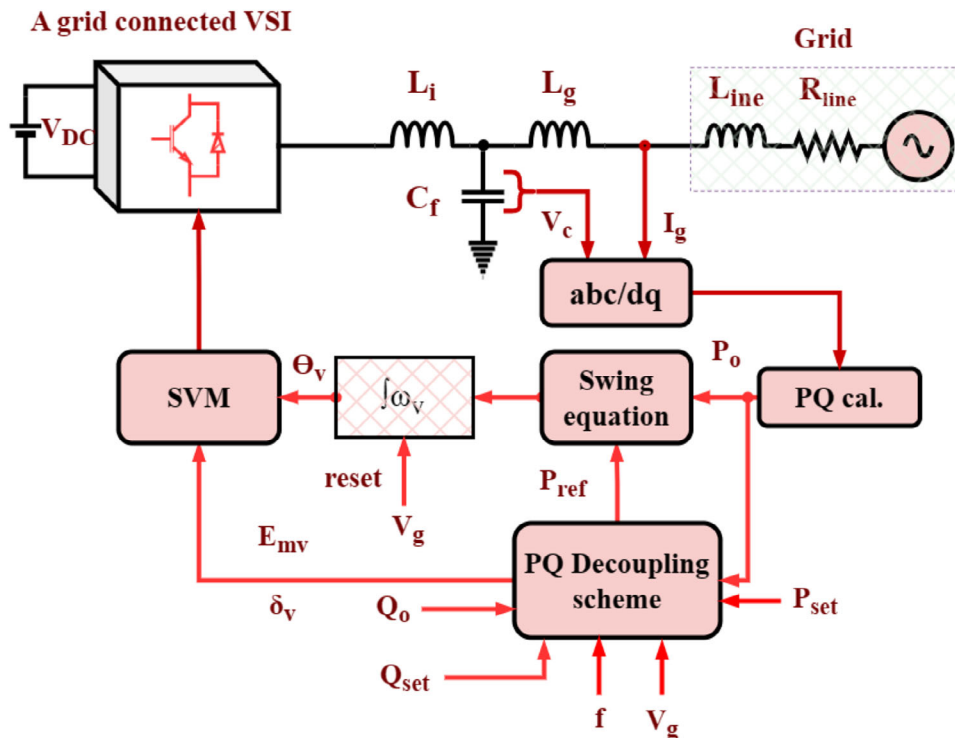
FIGURE 7 A considered grid connected synchronverter system for simulation studies.
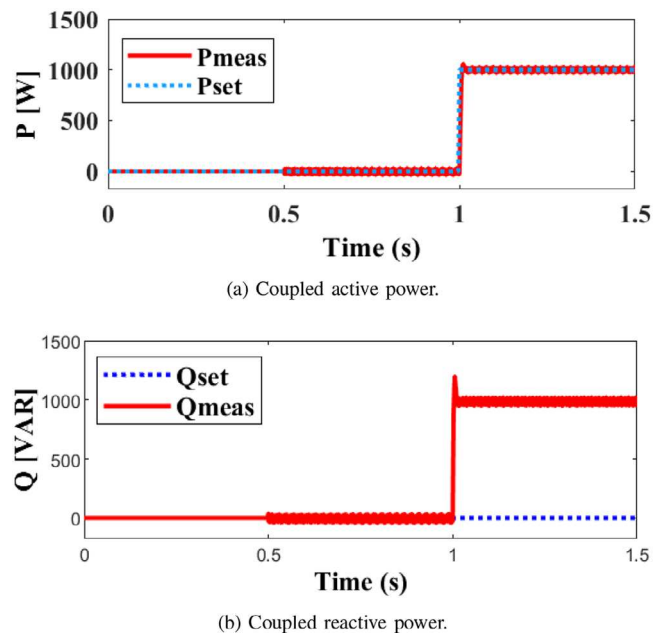

(a) Coupled active power.

(b) Coupled reactive power.

FIGURE 8 A coupled PQ control. The supplied Q increases away from its setpoint when the supplied P increments to its new setpoint.

$t = 1$ s, thence to 4000 W at $t = 1.5$ s, and finally to 500 W at $t = 2$ s.

It is shown in Figure 9a that the measured P follows its reference at all times but the measured Q deviates when P exceeds 1000 W. Therefore, there is partial PQ decoupling with $\gamma = 1$. It is also observed that the impact of adding virtual decoupling

impedance is on the voltage applied to the inverter. Figure 9c shows that the required RMS voltage changes to 244.2 V, 256.5 V and 242.1 V at the respective times corresponding to a step change in P. Therefore, the addition of negative resistance increases the voltage demand from the inverter, and the values of the virtual impedance must be carefully designed so that the increase in voltage by virtual impedance does not cause the applied voltage to exceed the specified standard voltage bounds. Moreover, the DC link must be designed to ensure that it is capable of supplying the required increase in voltage.

5.3 | Total decoupled PQ control ($\gamma = 0.04$)

This case describes the total PQ decoupling by the proposed scheme which is achieved when $\gamma = 0.04$. A system is initialised and synchronised to the grid at around 0.5 s. The ability to decouple P and Q and achieve their independent control is shown in Figures 10a and 10b. A step change of P is invoked from 0 to 1000 W at $t = 1$ s, followed by changes to 4000 W and 500 W at times $t = 1.5$ s and $t = 2$ s, respectively. Both the measured P and Q follow their references successfully during this time. A step change in Q is then introduced from 0 to 500 var at time $t = 2.5$ s; this is done to demonstrate that both P and Q can change independently. The measured Q follows its reference successfully while P still tracks its reference.

In both Figures 10a and 10b, transients occur in the P and Q variables when the other variable changes. These are due to the decoupling action and last for less than one quarter of the power
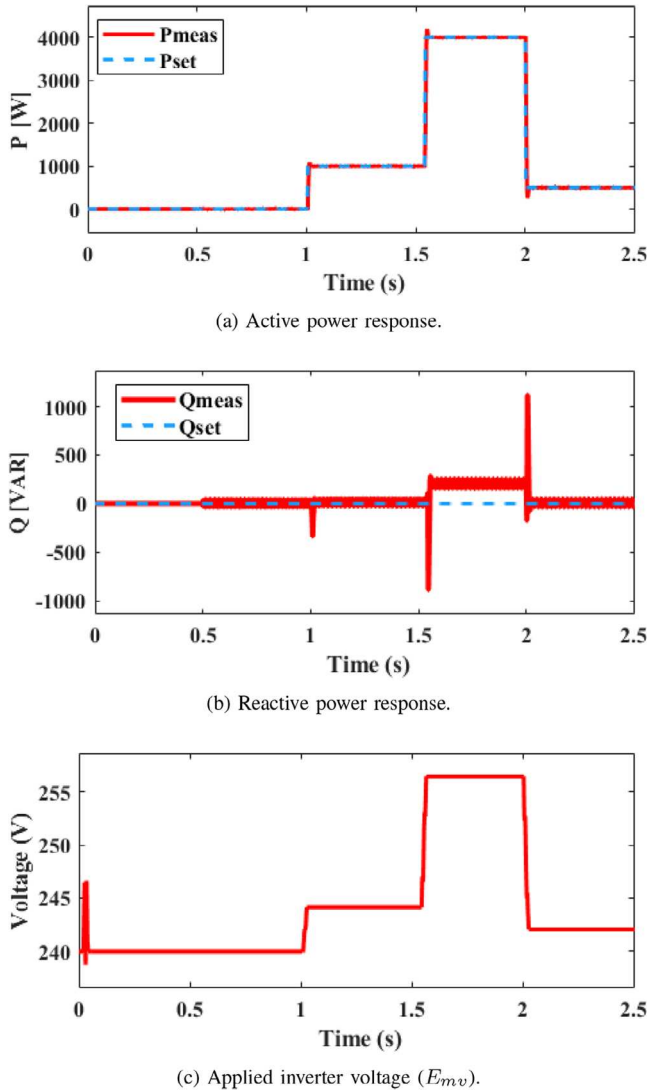
(a) Active power response.

(b) Reactive power response.

(c) Applied inverter voltage (E_{mv}).

FIGURE 9 Partial PQ decoupling (with $\gamma = 1$). The active power P follows its setpoint while smaller deviations in Q result.

(a) Active power response.

(b) Reactive power response.

(c) Applied inverter voltage (E_{mv}).

FIGURE 10 Total PQ decoupling ($\gamma = 0.04$). Both P and Q follow their setpoints.

frequency cycle; hence, they would not be expected to interfere with the normal sychronverter operations. Since addition of the *RCL* decoupling circuit places demands on the required inverter voltage, it is important to analyse the magnitude of voltages required when changes of both P and Q are invoked. In Figure 10c, it is shown that the voltage required is within 10% of the nominal voltage, which is a standard for many distribution voltages. The maximum RMS voltage change from the nominal value is +7.1% (from 240 V to 257 V).

Finally, THD analysis was performed for each current section during P and Q variations. According to IEEE 1547 standard [32], the THD of the injected current by the grid-connected inverter must be below 5%. It is shown in Figure 11 that the THD for each current section is below this specified value: the typical values of THS are 1.05%, 0.22% and 1.87% for the different P values (with $Q = 0$) of 1000 W, 4000 W W and 500 W, respectively; on the other hand, the THD was 1.49% when P was set to 500 W and Q to 500 var.
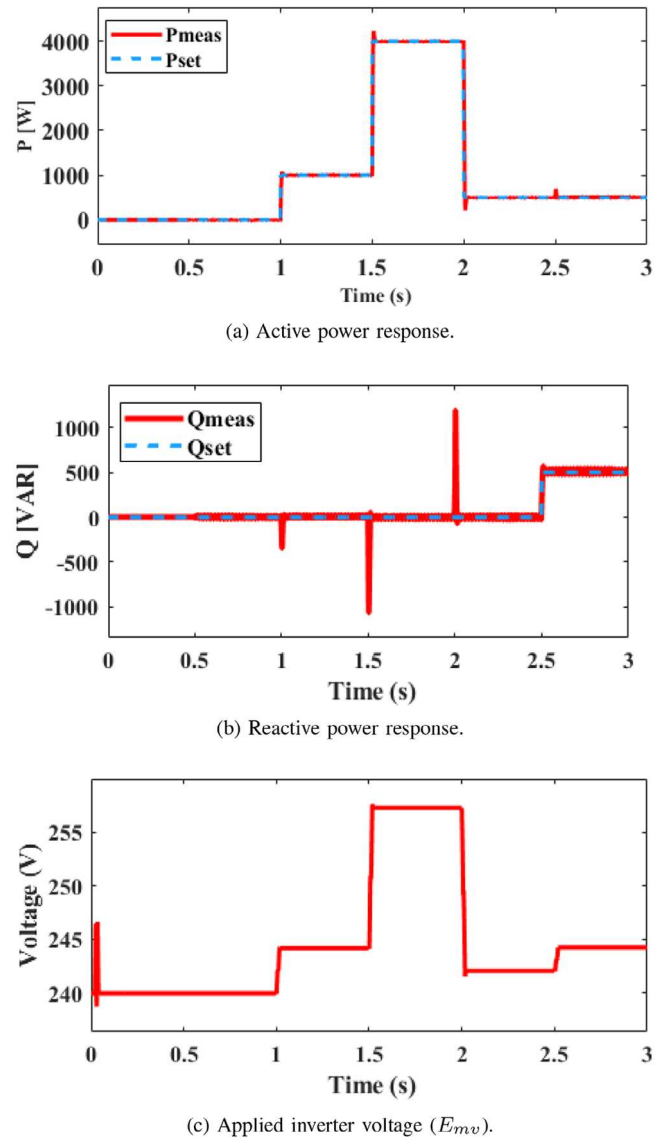
5.4 | Response under grid frequency variations

This fourth case aims to analyse the response of the modified synchronverter when there are frequency variations in the weak grid. A totally decoupled synchronverter ($\gamma = 0.04$) is used. Similar to the previous cases, the synchronverter is initialized and synchronized to the grid at around $t = 0.5$ s.

A step change in P, from 0 to 1000 W, is commanded at $t = 1$ s, followed by a step change in Q, from 0 to 200 var, at $t = 1.5$ s. This is important to invoke normal operation of the synchronverter at its limits before the insertion of frequency variations.

It can be observed from Figures 12a and 12b that, prior to the imposed frequency drop, $P_{set} = P_{ref}$ and $Q_{set} = Q_{ref}$. That is, there is no droop action and, hence, the grid frequency and voltage are at their desired nominal values. At $t = 2$ s, a grid
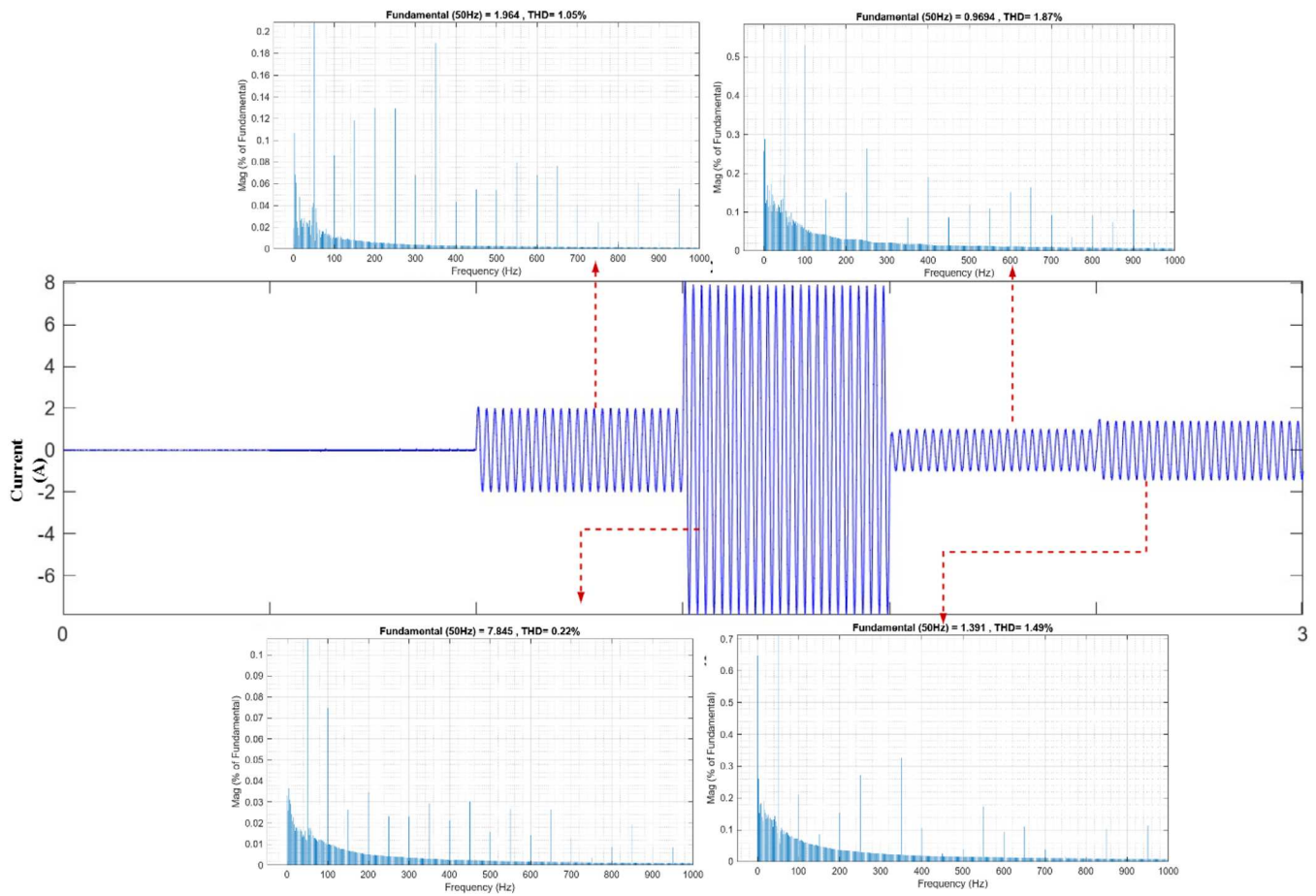
FIGURE 11 A THD analysis for the grid injected current.

frequency drop of 0.2% is simulated. The grid recovers after 25 power frequency cycles, as shown in Figure 12c. During this time, the synchronverter remains synchronized with the grid without producing large grid currents (Figure 12d).

Similarly, the synchronverter continues to supply power while helping the grid to recover to its nominal grid frequency. This is achieved by increasing the P supplied such that the $P_{ref} > P_{set}$ (Figure 12a); the size of increase in P_{ref} depends on the value of the droop coefficient D_p. After the grid frequency recovery, the synchronverter adjusts the supplied additional P, which was for frequency recovery, to its setpoint such that $P_{set} = P_{ref}$ again. The measured Q follows its reference value albeit for some transients during P changes due to the decoupling actions. The synchronverter manages to track grid frequency without losing synchronism (Figure 12c).

5.5 | Response under grid voltage variations

The final case aims to validate the ability of the modified synchronverter to aid the grid recovering to its nominal voltage in the event mild grid voltage variations. Similar to Section 5.4, a decoupled synchronverter ($\gamma = 0.04$) is initialized and synchronized to the grid at around 0.5 s, and the same P and Q changes

are invoked at the same times seen in the previous case. A voltage sag of 90% is simulated at $t = 2$ s, from which the grid recovers to its nominal RMS voltage after 25 power frequency cycles (Figure 13e). In Figure 13a we see that the P supply is maintained at all times, with $P_{set} = P_{ref}$ because of the absence of frequency variables.

Figure 13b provides the Q response under this scenario. After the insertion of the grid voltage variation at $t = 2$ s, the generated Q is increased by the droop controller, necessary to aid the voltage recovery in the grid. This increase is maintained until the grid voltage recovers to its nominal value at around $t = 2.5$ s.

During the voltage step change, there is an surge of grid current (Figure 13d). The magnitude of this transient current, however, is less than 2 per units of the nominal rating grid current, as can be observed in zoomed in phase A current in Figure 13d; therefore, the transient current is within the typical safe operating region of the semiconductor devices.

6 | CONCLUSION

A virtual shifting of the centre of the PQ-power circle and its corresponding radius modulation has been presented, to
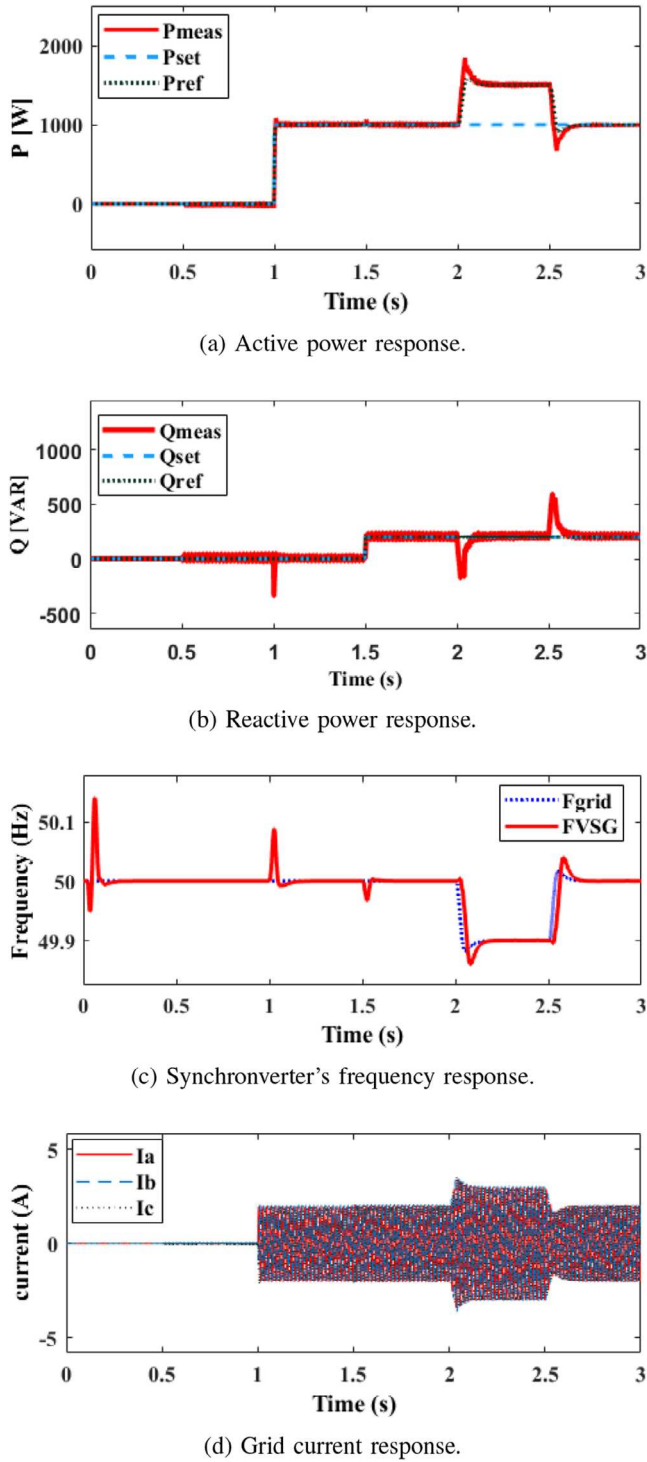
(a) Active power response.

(b) Reactive power response.

(c) Synchronverter's frequency response.

(d) Grid current response.

FIGURE 12 System response under 0.2% grid frequency drop.

(a) Active power response.

(b) Reactive power response.

(c) Synchronverter's frequency response

(d) Grid current response.

(e) Grid voltage response.

FIGURE 13 System response under a voltage sag of 90%.

achieve decoupled *PQ* control for a VSG connected to the weak grid. Implementation of the scheme and simulations were provided to demonstrate its validity. Using this technique a VSG such as a synchronverter connected to the weak grid can achieve a decoupled *PQ* control such that it can be controlled as a typical SG connected to a strong grid. This is achieved with simplicity in quantification of the type and their corresponding
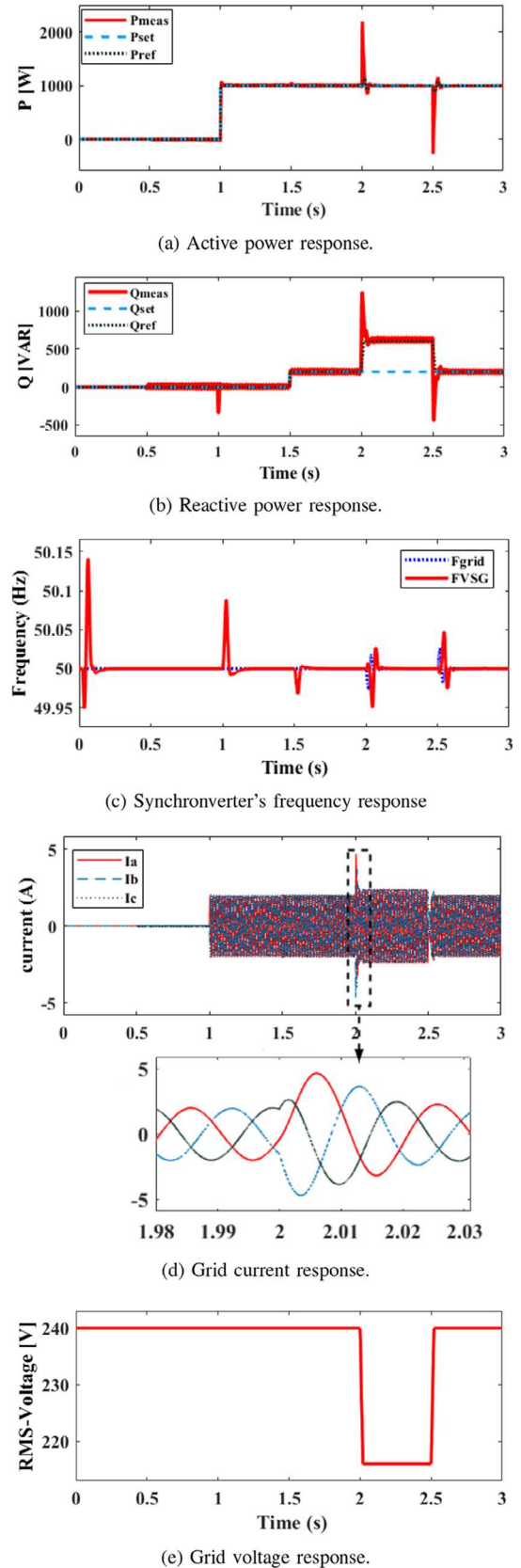
required magnitudes of the virtual impedance. Moreover, the presented scheme adapts to the stochasticity of both loads and RES such that it achieves PQ decoupling with the abrupt change in power demand, which is likely in a weak grid, as presented in the simulation results. Furthermore, the VSG can aid the grid recovering to its nominal frequency and voltage in case of their mild variations.

The proposed approach assumes knowledge of grid impedance; in a practical weak-grid setting this may necessitate the online estimation of impedance. The presented study also considers a balanced grid—future work will consider unbalanced grids—and mild voltage variations rather than severe faults. The issue with the latter is that the addition of a series capacitor lowers the VSG-to-grid interfacing impedance, so that high currents might result on occurrence of severe faults. The proposed approach therefore requires a low voltage ride through technique (LVRT) to be coordinated with the scheme during faults. As future work will show, this can be achieved by augmenting the modified synchronverter with superconductor fault current limiters (SFCLs). Moreover, the use of an active SFCL can aid grid balancing in the event of unbalanced conditions.

NOMENCLATURE

γ	A virtual power circle identifier
δ	Power angle
θ	Phase angle of the grid voltage
D_p	Active power droop gain
D_q	Reactive power droop gain
E	Internal voltage of the VSG
P	Active power
P_{ref}	Reference active power
P_{set}	Set active power
P_0	Measured active power
Q	Reactive power
Q_{ref}	Reference reactive power
Q_{set}	Set reactive power
Q_0	Measured reactive power
R	Resistance
R_v	Virtual resistance
V_g	Grid voltage
X	Reactance
X_{Lv}	Virtual inductive reactance
X_v	Virtual capacitive impedance
Z	Impedance
Z_s	Impedance between synchronous generator and strong grid

AUTHOR CONTRIBUTIONS

Daniel Angelo Kisinga: Conceptualization; formal analysis; investigation; software; writing—original draft; writing—review & editing. **Peter Makolo**: Writing—review & editing. **Paul Trodden**: Supervision; validation; writing—review & editing.

CONFLICT OF INTEREST STATEMENT

The authors declare no conflict of interest.

DATA AVAILABILITY STATEMENT

Data sharing not applicable to this article as no specific datasets were generated or analyzed during the current study.

ORCID

Daniel Angelo Kisinga https://orcid.org/0000-0002-0281-6623

Peter Makolo https://orcid.org/0000-0002-3595-8468

REFERENCES

1. International Renewable Energy Agency (IRENA): Smart Electrification with Renewables: Driving the Transformation of Energy Services. IRENA, London (2022)
2. Makolo, P., Zamora, R., Lie, T.-T.: The role of inertia for grid flexibility under high penetration of variable renewables-a review of challenges and solutions. Renewable Sustainable Energy Rev. 147, 111223 (2021)
3. Homan, S., Mac Dowell, N., Brown, S.: Grid frequency volatility in future low inertia scenarios: Challenges and mitigation options. Appl. Energy 290, 116723 (2021)
4. Kisinga, D.A., Makolo, P., Trodden, P.A.: A neural network-based online estimation of stochastic inertia in a power system. 2022 IEEE PES/IAS Power-Africa, pp. 1–5. IEEE, Piscataway (2022)
5. Beck, H.-P., Hesse, R.: Virtual synchronous machine. In: 2007 9th international conference on electrical power quality and utilisation, pp. 1–6. IEEE, Piscataway (2007)
6. Zhong, Q.-C., Weiss, G.: Synchronverters: Inverters that mimic synchronous generators. IEEE Trans. Ind. Electron. 58(4), 1259–1267 (2010)
7. Sakimoto, K., Miura, Y., Ise, T.: Stabilization of a power system with a dis-tributed generator by a virtual synchronous generator function. In: 8th Inter-national Conference on Power Electronics-ECCE Asia, pp. 1498–1505. IEEE, Piscataway (2011)
8. Hou, X., Han, H., Zhong, C., Yuan, W., Yi, M., Chen, Y.: Improvement of transient stability in inverter-based AC microgrid via adaptive virtual inertia. In: 2016 IEEE Energy Conversion Congress and Exposition (ECCE), pp. 1–6. IEEE, Piscataway (2016)
9. Zhong, C., Li, H., Zhou, Y., Lv, Y., Chen, J., Li, Y.: Virtual synchronous generator of PV generation without energy storage for frequency support in autonomous microgrid. Int. J. Electr. Power Energy Syst. 134, 107343 (2022)
10. Hou, X., Sun, Y., Zhang, X., Lu, J., Wang, P., Guerrero, J.M.: Improvement of frequency regulation in VSG-based AC microgrid via adaptive virtual inertia. IEEE Trans. Power Electron. 35(2), 1589–1602 (2019)
11. Tamrakar, U., Shrestha, D., Maharjan, M., Bhattarai, B.P., Hansen, T.M., Tonkoski, R.: Virtual inertia: Current trends and future directions. Appl. Sci. 7(7), 654 (2017)
12. Yu, F., Booth, C., Dy sko, A.: Backup protection requirements in future low-inertia power systems. In: 2016 51st International Universities Power Engineering Conference (UPEC), pp. 1–6. IEEE, Piscataway (2016)
13. NationalGridESO: What is short circuit level. https://www.nationalgrideso.com/news/what-short-circuit-level. Accessed Dec 2021.
14. Asrari, A., Mustafa, M., Ansari, M., Khazaei, J.: Impedance analysis of virtual synchronous generator-based vector controlled converters for weak AC grid integration. IEEE Trans. Sustainable Energy 10(3), 1481–1490 (2019)

15. Shintai, T., Miura, Y., Ise, T.: Oscillation damping of a distributed generator using a virtual synchronous generator. IEEE Trans. Power Delivery 29(2), 668–676 (2014)

16. Li, B., Zhou, L., Yu, X., Zheng, C., Liu, J.: Improved power decoupling control strategy based on virtual synchronous generator. IET Power Electron. 10(4), 462–470 (2017)

17. Li, G., Ma, F., Luo, A., He, Z., Wu, W., Wei, X., Zhu, Z., Guo, J.: Virtual impedance-based virtual synchronous generator control for grid-connected inverter under the weak grid situations. IET Power Electron. 11(13), 2125–2132 (2018)

18. Zhang, P., Zhao, H., Cai, H., Shi, J., He, X.: Power decoupling strategy based on 'virtual negative resistor' for inverters in low-voltage microgrids. IET Power Electron. 9(5), 1037–1044 (2016)

19. Abusara, M.A., Guerrero, J.M., Sharkh, S.M.: Line-interactive UPS for microgrids. IEEE Trans. Ind. Electron. 61(3), 1292–1300 (2013)

20. Pan, H., Wei, T., Deng, C., Long, H., Zhang, Y.: A novel PQ control strategy for non phase-locked loop based on hilbert transform. In: 2018 IEEE Energy Conversion Congress and Exposition (ECCE), pp. 2676–2682. IEEE, Piscataway (2018)

21. Chen, Y., Zhao, J., Wang, J., Qu, K., Ushiki, S., Ohshima, M.: A decupled PQ control strategy of voltage-controlled inverters. In: 2015 9th International Conference on Power Electronics and ECCE Asia (ICPE-ECCE Asia), pp. 1374–1379. IEEE, Piscataway (2015)

22. Chen, Y., Zhao, J., Qu, K., Li, F.: PQ control of micro grid inverters with axial voltage regulators. J. Power Electron. 15(6), 1601–1608 (2015)

23. Lu, X., Wang, J., Guerrero, J.M., Zhao, D.: Virtual-impedance-based fault current limiters for inverter dominated AC microgrids. IEEE Trans. Smart Grid 9(3), 1599–1612 (2016)

24. Natarajan, V., Weiss, G.: Synchronverters with better stability due to virtual inductors, virtual capacitors, and anti-windup. IEEE Trans. Ind. Electron. 64(7), 5994–6004 (2017)

25. Zheng, C., Dragičević, T., Blaabjerg, F.: Model predictive control-based virtual inertia emulator for an islanded alternating current microgrid. IEEE Trans. Ind. Electron. 68(8), 7167–7177 (2020)

26. Çelik, D., Meral, M.E.: A coordinated virtual impedance control scheme for three phase four leg inverters of electric vehicle to grid (V2G). Energy 246, 123354 (2022)

27. Astrada, J., De Angelo, C.: Double virtual-impedance loop for inverters with repetitive and droop control in UPS applications. Electr. Power Syst. Res. 204, 107680 (2022)

28. Çelik, D., Meral, M.E.: A coordinated virtual impedance control scheme for three phase four leg inverters of electric vehicle to grid (v2g). Energy 246, 123354 (2022)

29. Dou, C., Zhang, Z., Yue, D., Song, M.: Improved droop control based on vir- tual impedance and virtual power source in low-voltage microgrid. IET Gener. Transm. Distrib 11(4), 1046–1054 (2017)

30. Fan, B., Li, Q., Wang, W., Yao, G., Ma, H., Zeng, X., Guerrero, J.M.: A novel droop control strategy of reactive power sharing based on adaptive virtual impedance in microgrids. IEEE Trans. Ind. Electron. 69(11), 11 335–11 347 (2021)

31. Guerrero, J.M., De Vicuna, L.G., Matas, J., Castilla, M., Miret, J.: Output impedance design of parallel-connected UPS inverters with wireless load-sharing control. IEEE Trans. Ind. Electron. 52(4), 1126–1135 (2005)

32. IEEE Application Guide for IEEE Std 1547, IEEE Standard for Interconnecting Distributed Resources With Electric Power Systems, IEEE Std 1547.2-2008 (2008)

33. Colombage, N.C.: Design and control of on-board bidirectional battery chargers with islanding detection for electric vehicle applications. Ph.D. Dissertation, University of Sheffield (2015)

34. Liu, F., Zhang, X., Yu, C., Shao, Z., Zhao, W., Ni, H.: LCL-filter design for grid-connected three-phase PWM converter based on maximum current ripple. In: 2013 IEEE ECCE Asia Downunder, pp. 631–635. IEEE, Piscataway (2013)

35. Liserre, M., Blaabjerg, F., Hansen, S.: Design and control of an LCL-filter-based three-phase active rectifier. IEEE Trans. Ind. Appl. 41(5), 1281–1291 (2005)

36. Xu, J., Xie, S., Huang, L., Ji, L.: Design of LCL-filter considering the control impact for grid-connected inverter with one current feedback only. IET Power Electron. 10(11), 1324–1332 (2017)

37. Dursun, M., DÖŞOĞLU, M.K.: LCL filter design for grid connected three phase inverter. In: 2018 2nd International Symposium on Multidisciplinary Studies and Innovative Technologies (ISMSIT), pp. 1–4. IEEE, Piscataway (2018)

38. Zhong, Q.-C., Nguyen, P.-L., Ma, Z., Sheng, W.: Self-synchronized synchronverters: Inverters without a dedicated synchronization unit. IEEE Trans. Power Electron. 29(2), 617–630 (2013)

How to cite this article: Kisinga, D.A., Makolo, P., Trodden, P.: A modified synchronverter for a weak grid with virtual power circles-based PQ decoupling scheme. IET Renew. Power Gener. 1–14 (2024). https://doi.org/10.1049/rpg2.13118